Available online at www.sciencedirect.com
ScienceDirect
Journal of Nuclear Materials 367–370 (2007) 556–560
journal of nuclear materials
www.elsevier.com/locate/jnucmat

A universal relationship between indentation hardness and flow stress

M.Y. He *, G.R. Odette, T. Yamamoto, D. Klingensmith

University of California, Santa Barbara, Materials Department, Santa Barbara, CA 93106-5050, USA

Abstract

A new indentation hardness (H) approach to evaluating the true stress (σ)–true plastic strain (ε) constitutive behavior of materials is described. Extensive elastic–plastic finite element (FE) simulations were carried out to assess the relation between H and $\sigma(\varepsilon)$. The analysis led to derivation of a *universal relation* between H and $\sigma(\varepsilon)$ given by $H \approx 4.05(1-34.6\ \sigma_{flow}/E)\sigma_{flow}$, where $\sigma_{flow} = \sigma_y + \langle\sigma_{sh}\rangle$, $\langle\sigma_{sh}\rangle$ is the average strain hardening between $\varepsilon = 0$ and 0.1, and E is the elastic modulus. Experimental H–σ_{flow} data pairs for the large set of alloys are in reasonably good agreement with the model predictions, but the experimental σ_{flow} are slightly higher and more linearly related to H than predicted. The H–σ_{flow} relation provides insight into the large variation of the H/σ_y ratios that are observed for different materials, as well as the corresponding variation in the $\Delta H/\Delta\sigma_y$ ratios used to estimate $\Delta\sigma_y$ due to changes in an alloy's condition, such as that induced by irradiation, based on measurements of ΔH. Notably, combinations of tensile and hardness tests can be use to estimate the average strain hardening from $\varepsilon = 0$ to 0.1 in irradiated alloys that have very small uniform strains.

1. Introduction

Micro-hardness (H) measurements provide a convenient, non-destructive means to evaluate the strength of materials [1,2], as well as to characterize strength changes, such as those due to irradiation hardening. A large number of finite element (FE) simulations of indentations and hardness have been reported (e.g., [3–13]). However the relation of H to more quantitative measures of true stress–strain $\sigma(\varepsilon)$ constitutive properties, such as the yield stress (σ_y) and post-yield strain hardening (σ_{sh}), have remained ambiguous, and to a large extent semi-empirical [11–13]. This is in large part due to the fact that H intrinsically probes a wide range of ε, hence, represents some '*average*' measure of an effective flow stress, $\sigma(\varepsilon) = \sigma_y + \sigma_{sh}$. The decomposition of $\sigma(\varepsilon)$ into σ_y and σ_{sh}, which is the appropriate physical form as proposed by Kocks and Mecking [14], provides a good basis from which to quantify the H–$\sigma(\varepsilon)$ relation. For a specified indentation geometry, from a continuum perspective the H–$\sigma(\varepsilon)$ relation can depend only on σ_y, σ_{sh} averaged over some undefined and perhaps variable ε-range, E (or the indenter and material modulus) and the friction coefficient, μ. For example, in the case of a perfectly plastic material, the H/σ_y ratio would be expected to depend only weakly on E and μ. Further, while indentations produce a large range of ε ($\approx$0 to 0.6), they are finite, and very small regions

* Corresponding author. Tel.: +1 805 893 7166; fax: +1 805 893 8486.
E-mail address: ming@engineering.ucsb.edu (M.Y. He).

0022-3115/$ - see front matter © 2007 Elsevier B.V. All rights reserved.
doi:10.1016/j.jnucmat.2007.03.044

of high ε would be expected to have little effect on σ_{sh} [13]. Thus we carried out an extensive series of finite element (FE) simulations of the relation between H and the flow stress σ_{flow} averaged over different ε ranges for a very wide range of $\sigma(\varepsilon)$ laws to assess the possibility of obtaining a more universal master H–$\sigma(\varepsilon)$ relation.

2. Finite element (FE) modeling of indentation hardness (H)

Cone indentations were simulated using the general purpose FE code ABAQUS [15]. The FE simulations accounted for large strain geometry changes experienced in indentation test and were based on J_2 flow theory and normality requirements in the associated flow rule. The cone indenter, with an angle of 68.2°, was treated as two-dimensional (z, r, symmetric in θ) rigid body. The two-dimensional half space mesh had 3021 four-node quadrilateral axisymmetric elements with 3232 nodes. The radial (r) and depth (z) dimensions of the mesh were $\approx 50\Delta_{max}$ and $20\Delta_{max}$, respectively, where Δ_{max} is the maximum penetration depth of the cone. The mesh was refined in the area under the indenter and there were more than 20 elements in the contact area under the indenter at maximum load. The calculations were carried out for a prescribed loading/unloading cycle to a maximum load, P. Hardness, H, was calculated as P/A, where A is the area of the permanent indentation, $\pi D^2/4$, where D is the diameter of the indentation referenced at the plane of the undeformed specimen surface. Test calculations were carried out to demonstrate that H was independent of the mesh size and a convergence study showed that the meshes provided accurate results for displacements and the pile-up profile. The H and pile-up shapes are insensitive to friction coefficients $\mu \geqslant 0.2$, which was used in the FE simulations. The calculated H values are also insensitive to the load P between 40 and 200 g.

One large set of simulations were carried out for $E = 200$ GPa and analytical constitutive laws in the form

$$\sigma(\varepsilon) = \sigma_y \quad \varepsilon \leqslant \varepsilon_y, \tag{1a}$$

$$\sigma(\varepsilon) = \sigma_y + \sigma_{sh} = \sigma_y + \sigma_{shm}[1 - \exp(-\gamma(\varepsilon - \varepsilon_y))] \quad \varepsilon > \varepsilon_y. \tag{1b}$$

Here, σ_{shm} is the maximum strain hardening and γ a parameter that describes the rate of approaching saturation. The H were calculated based on Eqs. (1) for a Luder's-yield strain ($\varepsilon_y = 0.005$) and a wide range of σ_y (100–850 MPa), maximum saturated strain hardening levels ($\sigma_{shm} = 125$–500) and pre-saturation hardening rates ($\gamma = 3$–15). The calculations were also carried out for actual $\sigma_{sh}(\varepsilon)$ curves derived from tensile tests on a large number of alloys with a very diverse range of constitutive properties ranging from: (a) annealed stainless steels with a low σ_y and a modest initial strain hardening rate along with a high σ_{shm}; (b) tempered martensitic steels with intermediate σ_y and a high σ_{shm} and strain hardening rate; (c) TiNb which has a low strain hardening rate. The materials modeled also

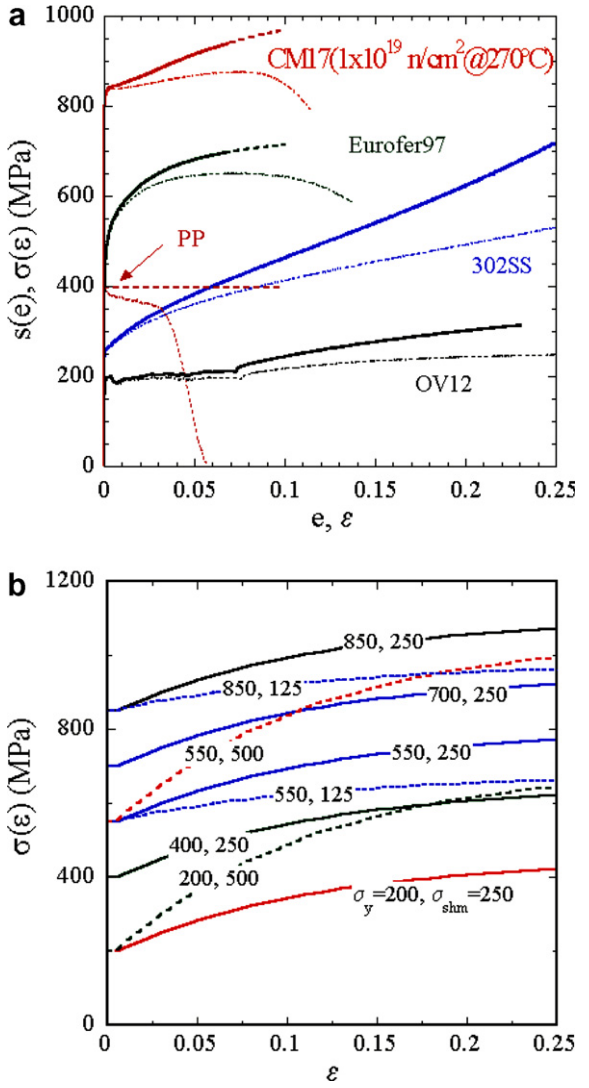

Fig. 1. Examples of the $\sigma(\varepsilon)$ functions used in the FE analysis: (a) experimentally derived curves and (b) analytical models. Note (a) also shows the engineering stress strain curves, $s(e)$.

included unirradiated and irradiated Mn–Mo–Ni reactor pressure vessel (RPV) steels, simple ferritic alloys, including some with very large Luders strain regions up to $\varepsilon_y \approx 0.1$ and pre-strained materials. Examples of the experimental and analytical $\sigma(\varepsilon)$ are shown in Fig. 1(a) and (b), respectively.

3. FE results and analysis

The initial FE calculations were done using $E = 200$ GPa, pertinent to steels. The FE H 'data' for the various $\sigma(\varepsilon)$ were analyzed by calculating the $\langle\sigma_{sh}\rangle$ between various lower (ε_l) and upper (ε_u) limits and fitting the corresponding $\sigma_{flow} = \sigma_y + \langle\sigma_{sh}\rangle$ versus H data with a function in the form

$$H = C_1(1 + C_2\sigma_{flow})\sigma_{flow}, \tag{2}$$

here C_1 and C_2 are functions of ε_l and ε_u. The optimum pair of ε_u and ε_l was determined by minimizing the standard deviation of the differences between the H predicted by Eq. (2) to the corresponding H data from the FE simulations for all the input $\sigma(\varepsilon)$. Values of $\varepsilon_l \approx 0.0$ and $\varepsilon_u \approx 0.1$ were found to give the best fit and in this case the H–σ_{flow} relation, shown as the fit line in Fig. 2, is give by

$$H = 4.05(1 - 34.6\sigma_{flow}/E)\sigma_{flow}. \tag{3}$$

This expression was originally derived for the set of analytical input $\sigma(\varepsilon)$, but Eq. (3) works equally well for the experimental $\sigma(\varepsilon)$. Fig. 2 also shows three-dimensional FE simulations for Vickers diamond pyramid hardness indentations (filled diamond symbols). The corresponding σ_{flow} data are slightly below the trend for the cone indentations at the higher H. We have also evaluated the effects of a non-rigid indentor, which are negligible. For example, for a perfect plastic material with yield stress 500 MPa, the H from FE simulation is 1859 MPa for $E = 200$ GPa indentor and 1855 MPa for a rigid indentor. Since it is the only other constitutive variable, the non-linearity in the H–σ_{flow} is expected to be due to the variation in σ_{flow}/E ratio. Fig. 3 shows H/σ_{flow} as a function of σ_{flow}/E (solid symbols): (a) for $E = 200$ GPa for various σ_y using the same $\sigma_{sh}(\varepsilon)$ (filled symbols); and, (b) for the same σ_y and $\sigma_{sh}(\varepsilon)$ and $E = 50$, 100, 200 and 400 GPa (open symbols). A polynominial fit to all the data yields the expression

$$H = 4.08(1 + 1755[\sigma_{flow}/E]^2 - 44.1[\sigma_{flow}/E])\sigma_{flow}. \tag{4}$$

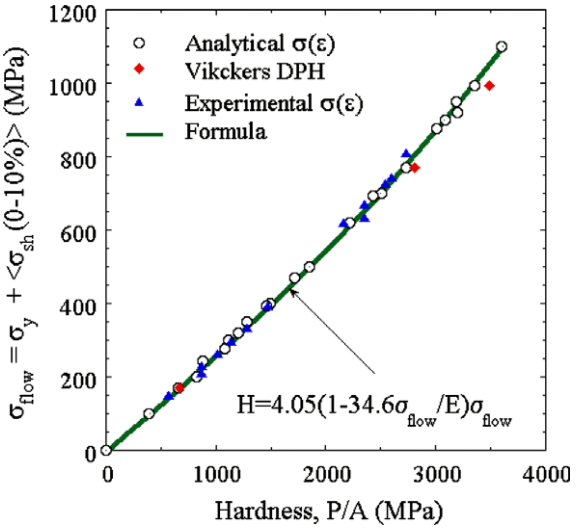

Fig. 2. The $\sigma_{flow} = \sigma_y + \langle\sigma_{sh}\rangle$ versus H for a wide range of $\sigma(\varepsilon)$ from the FE simulations. The filled diamond symbols are for 3D FE calculations for Vickers diamond pyramid hardness indentations. All others are for the 2D cone indentations.

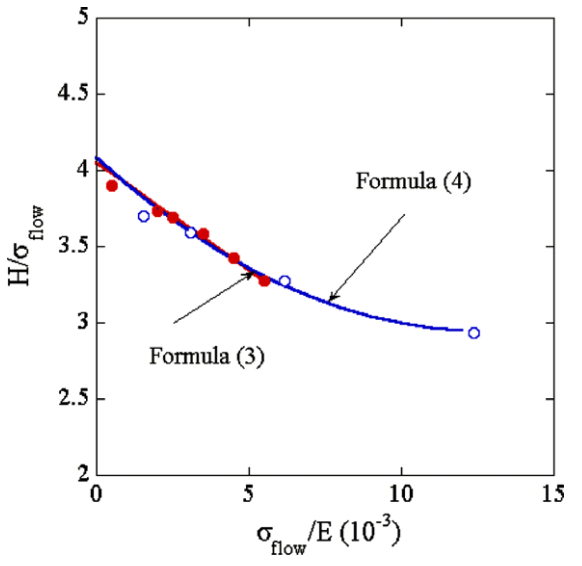

Fig. 3. The calculated σ_{flow}/H versus σ_{flow}/E and the corresponding fitting functions.

However, for most materials of interest σ_{flow}/E is <0.006, and, fitting the σ_{flow}/E versus σ_{flow}/E data in this range is adequately represented by a simple linear relation in Eq. (3). Note, the expressions for H as a function σ_{flow} can be readily inverted to give σ_{flow} as a function of H.

4. Comparison with experiment

Coupled tensile and Vickers diamond pyramid hardness (DPH) tests were carried out on a large number of alloys with a very diverse range of $\sigma(\varepsilon)$. As noted previously, the alloys included: (a) annealed stainless steel, copper and brass with high strain hardening; (b) TiNb with low strain hardening rates; (c) unirradiated and irradiated pressure vessel steels and simple ferritic alloys; (d) prestrained alloys; and, (e) a Fe–N alloys with a very large Luders strain. The $\sigma_{\text{flow}} = \sigma_y + \langle\sigma_{sh}\rangle$ were directly assessed based on the experimental $\sigma_{sh}(\varepsilon) = \sigma(\varepsilon) - \sigma_y$ data averaged between $\varepsilon = 0$ and 0.1, derived from engineering stress strain curves up to the onset of necking. In cases where the experimental $\sigma(\varepsilon)$ did not reach $\varepsilon = 0.1$, the data were extrapolated based on the Kocks and Mecking model [14]. The TiNb was assumed to be perfectly plastic.

Fig. 4 compares the experimental H–σ_{flow} data pairs to the predictions of Eq. (3). The agreement is reasonably good, although the experimental σ_{flow} data tend to fall slightly above the prediction line as shown by the dashed best fit line, that is given by the expression in consistent units of MPa as

$$\sigma_{\text{flow}} = 1.72 \times 10^{-7} H^2 + 0.272H. \tag{5}$$

The differences between the experimental DPH based H–σ_{flow} curves and that predicted by the FE model cannot be understood on the basis of geometric variations. Note, the predicted curve in Fig. 4 is for $E = 200$ MPa (since most of the data is for steels and iron based alloys), thus it does not fully account for elastic modulus variations in the experimental data. However, the differences ($\approx$5% at $H =$ 2000 MPa) are small and could arise from minor effects, such as that due to strain gradient plasticity [9,10], which are not accounted for in the model.

Indeed, considering the uncertainties in the data, and simplicity of the model, we believe the agreement between the experimental observations and the FE based universal H–σ_{flow} relation is remarkably good.

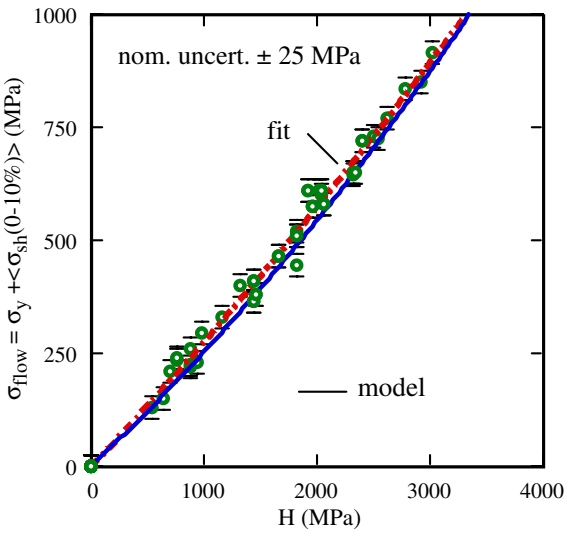

Fig. 4. Pairs of experimental σ_{flow}–H data points for a variety of metals and alloys with a wide range of $\sigma(\varepsilon)$ compared to the FE model prediction. The dashed line is a least square fit to the data.

5. Discussion

The universal master H–σ_{flow} relation is somewhat surprising in view of the much larger ε-range created by an indentation as illustrated in Fig. 5. We do not have a quantitative explanation why the ε-range from 0 to 0.1 is optimal to average a σ_{flow} that correlates with H. However, qualitatively it is clear from Fig. 5, that the volume of plastically strained material decreases rapidly with increasing ε. The total plastic work is determined by the volume weighted plastic work W given by

$$W = \int\int \sigma_{\text{flow}}(\varepsilon)\mathrm{d}\varepsilon\,\mathrm{d}V. \tag{6}$$

This implies that a finite, but limited range of ε, makes the predominant contributions to the net H. Thus, at this point the universal master H–σ_{flow} relation must be viewed as a useful empirical approximation. However, it permits a quantitative

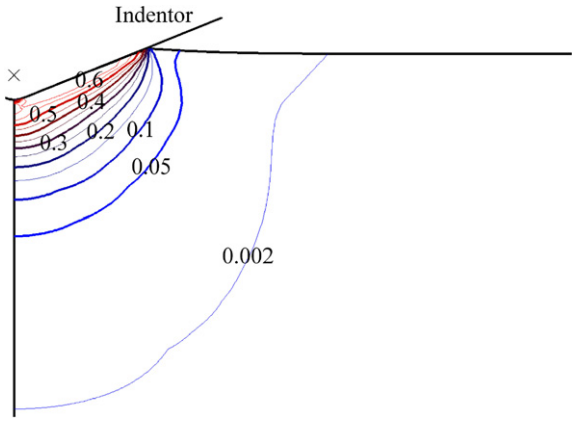

Fig. 5. A typical effective strain distribution under the indenter.

understanding of a number of empirical trends. These include

1. The large variation in the observed hardness to yield stress (H/σ_y) ratios in various alloys is due to the effects of differences in both $\langle\sigma_{sh}\rangle$ and, to a lesser extent, the σ_{flow}/E ratio. For example, in the limiting cases of $\sigma_y = 0$ and finite σ_{sh}, H/σ_y would be infinite. Further, the ratio of H/σ_y tends to be higher for alloys with low $\langle\sigma_{flow}\rangle$ due to the lower σ_{flow}/E.
2. The $\Delta H/\Delta\sigma_y$ following irradiation is generally lower than the unirradiated H/σ_y, primarily due to reduction in $\langle\sigma_{sh}\rangle$, and to a lesser extent the effect of the higher σ_{flow}/E ratio.

In addition, the universal relation allows combining H and σ_y measurements from a tensile test to estimation of strain hardening in alloys with very low or no uniform tensile strain as:

$$\langle\sigma_{sh}\rangle = \sigma_{flow}\ (\text{from } H) - \sigma_y\ (\text{from a tensile test}). \tag{7}$$

The universal relation also permits a convenient method to evaluate $\sigma(\varepsilon)$ at high ε regions by making H measurements on pre-strained materials. An effective way to do this is to make hardness transverses across sections of a bent beam that undergoes stable plastic deformation over a wide range of effective ε. Indeed, such transverses can also provide information on differences in $\sigma(\varepsilon)$ for tension versus compression loading.

6. Concluding remarks

Finite element simulations were carried out for a wide variety of analytical and experimental $\sigma(\varepsilon)$ to derive a *universal relation* between H and σ_{flow}, given by $H \approx 4.05(1–34.6\sigma_{flow}/E)\sigma_{flow}$, where σ_{flow} is the average flow stress between $\varepsilon = 0$ and 0.1. Experimental H–σ_{flow} data pairs are in good agreement with the model predictions. The H–σ_{flow} relation provides insight into the large variations in the H/σ_y and $\Delta H/\Delta\sigma_y$ ratios observed for different alloys and alloy conditions. Further, combinations of tensile and hardness tests can be used to estimate average strain hardening from 0 to 0.1 in irradiated alloys that have very small uniform tensile strains.

Acknowledgements

The work was supported by the US Department of Energy, Office of Fusion Science (Grant #DE-FG03-94ER54275). The authors gratefully acknowledge reviewers for their helpful suggestions.

References

[1] K.L. Johnson, Contact Mechanics, Cambridge University, 1985.
[2] K.L. Johnson, J. Mech. Phys. Solids 18 (1970) 115.
[3] S. Shim, W.C. Oliver, G.M. Pharr, in: Fundamentals of Nanoindentation and Nanotribology III. MRS Symposium Proceedings Series 841 (2005) 39.
[4] H. Lee, S. Jeong, Thin Solid Films 1–2 (2005) 173.
[5] L. Wang, M. Ganor, S.I. Rokhlin, J. Mater. Res. 20 (2005) 987.
[6] Y. Choi, B. Lee, H. Lee, D. Kwon, in: Thin Films – Stresses and Mechanical Properties, MRS Symposium Proceedings Series 795 (2004) 339.
[7] M. Sakai, T. Akatsu, S. Numata, Acta Mater. 52 (2004) 2354.
[8] M. Mata, J. Alcala, J. Mech. Phys. Solids 52 (2004) 145.
[9] A.A. DiCarlo, H.T.Y. Yang, S. Chandrasekar, in: Nano- and Microelectromechanical Systems (NEMS and MEMS) and Molecular Machines, MRS Symposium Proceedings Series 741 (2003) 157.
[10] Y. Wei, J.W. Hutchinson, J. Mech. Phys. Solids 51 (2003) 2037.
[11] C. Santos, G.R. Odette, G.E. Lucas, T. Yamamoto, J. Nucl. Mater. 258 (1998) 452.
[12] M.Y. He, G.R. Odette, G.E. Lucas, in: Fundamentals of Nanoindentation II, MRS Symposium Proceedings Series 649 (2001) Q7.9.
[13] M.Y. He, G.R. Odette, G.E. Lucas, B. Schroeter, Small Specimen Test Techniques-IV, ASTM STP 1418 (2002) 306.
[14] H. Mecking, U.F. Kocks, Acta Metall. 29 (1981) 1865.
[15] ABAQUS USER'S Manual, Version 6.3, Hibbitt, Karlsson and Sorensen Inc., 2002.